

---

21 Jan 2022

## Characterization of Single-Shot Attosecond Pulses with Angular Streaking Photoelectron Spectra

Xi Zhao

Siqi Li

Taran Driver

Van Hung Hoang

*et. al.* For a complete list of authors, see [https://scholarsmine.mst.edu/phys\\_facwork/2211](https://scholarsmine.mst.edu/phys_facwork/2211)

Follow this and additional works at: [https://scholarsmine.mst.edu/phys\\_facwork](https://scholarsmine.mst.edu/phys_facwork)

 Part of the [Physics Commons](#)

---

### Recommended Citation

X. Zhao et al., "Characterization of Single-Shot Attosecond Pulses with Angular Streaking Photoelectron Spectra," *Physical Review A*, vol. 105, no. 1, article no. 013111, American Physical Society (APS), Jan 2022.

The definitive version is available at <https://doi.org/10.1103/PhysRevA.105.013111>

This Article - Journal is brought to you for free and open access by Scholars' Mine. It has been accepted for inclusion in Physics Faculty Research & Creative Works by an authorized administrator of Scholars' Mine. This work is protected by U. S. Copyright Law. Unauthorized use including reproduction for redistribution requires the permission of the copyright holder. For more information, please contact [scholarsmine@mst.edu](mailto:scholarsmine@mst.edu).

**Characterization of single-shot attosecond pulses with angular streaking photoelectron spectra**Xi Zhao<sup>1</sup>, Siqi Li<sup>2,3</sup>, Taran Driver<sup>2,3</sup>, Van-Hung Hoang<sup>1</sup>, Anh-Thu Le<sup>4</sup>, James P. Cryan<sup>2,3</sup>, Agostino Marinelli<sup>2,3</sup> and C. D. Lin<sup>1,\*</sup><sup>1</sup>*Department of Physics, Kansas State University, Manhattan, Kansas 66506, USA*<sup>2</sup>*SLAC National Accelerator Laboratory, Menlo Park, California 94025, USA*<sup>3</sup>*Stanford PULSE Institute, SLAC National Accelerator Laboratory, Menlo Park, California 94025, USA*<sup>4</sup>*Department of Physics, Missouri University of Science and Technology, Rolla, Missouri 65409, USA*

(Received 6 April 2021; revised 12 August 2021; accepted 13 August 2021; published 21 January 2022)

Most of the traditional attosecond pulse retrieval algorithms are based on a so-called attosecond streak camera technique, in which the momentum of the electron is shifted by an amount depending on the relative time delay between the attosecond pulse and the streaking infrared pulse. Thus, temporal information of the attosecond pulse is encoded in the amount of momentum shift in the streaked photoelectron momentum spectrogram  $S(p, \tau)$ , where  $p$  is the momentum of the electron along the polarization direction and  $\tau$  is the time delay. An iterative algorithm is then employed to reconstruct the attosecond pulse from the streaking spectrogram. This method, however, cannot be applied to attosecond pulses generated from free-electron x-ray lasers where each single shot is different and stochastic in time. However, using a circularly polarized infrared laser as the streaking field, a two (or three)-dimensional angular streaking electron spectrum can be used to retrieve attosecond pulses for each shot, as well as the time delay with respect to the circularly polarized IR field. Here we show that a retrieval algorithm previously developed for the traditional streaking spectrogram can be modified to efficiently characterize single-shot attosecond pulses. The methods have been applied to retrieve 188 single shots from recent experiments. We analyze the statistical behavior of these 188 pulses in terms of pulse duration, bandwidth, pulse peak energy, and time delay with respect to the IR field. The retrieval algorithm is efficient and can be easily used to characterize a large number of shots in future experiments for attosecond pulses at free-electron x-ray laser facilities.

DOI: [10.1103/PhysRevA.105.013111](https://doi.org/10.1103/PhysRevA.105.013111)**I. INTRODUCTION**

The motion of electrons in molecules and solids occurs on the subfemtosecond timescale [1]. To probe these dynamics with atomic-site specificity requires light pulses from the soft x-ray (SXR) spectral region and beyond [2–10]. Consequently, to study or control ultrafast electronic phenomena requires attosecond x rays that can interact with the core levels of the target [11]. Two approaches for the generation of x-ray attosecond pulses have been developed in recent years. One is based on high-order-harmonic generation (HHG) using midinfrared lasers, with wavelengths of 2  $\mu\text{m}$  and longer [12–17]. The other is x-ray free-electron laser (XFEL) facilities, such as the Linac Coherent Light Sources (LCLS) [15]. The working principle of HHG is the rescattering process, where an intense infrared laser field is used to drive electrons coherently in an atom or molecule. Within an optical cycle, as the accelerated electrons return to recombine with the parent ion, up-conversion with emitted light reaching soft x rays is achieved if the returning electrons gain kinetic energies up to hundreds of electron volts (eV) [12–14]. To reach such high energies, midinfrared driving lasers are used as the returning kinetic energy is proportional to the square of the wavelength of the fundamental laser. In the case of XFELs, soft x-ray

pulses are generated through the interaction of a relativistic electron beam with an x-ray electric field in a long undulator which consists of a periodic array of magnetic dipoles. As the electrons pass through the magnetic device, they oscillate and emit radiation. The emitted radiation feeds back on the electron bunch, inducing a microbunching. This microbunching structure leads to coherent emission of x rays with very high peak power [15].

For time-resolved pump-probe experiments, single isolated attosecond pulses (IAPs) are preferred. For such a pulse with duration of approximately 100 as, the spectral full width at half maximum (FWHM) bandwidth is about 20 eV. For a duration down to 10 as, the bandwidth would be 200 eV. However, knowledge of the bandwidth alone cannot tell the pulse duration. To know the electric field in the time domain, the spectral phase must also be determined. Historically, high-order-harmonic spectra have been generated since the late 1980s, but the phases of harmonics were not determined until 2001 [18]. The success of spectral phase determination in 2001 thus marked the beginning of attosecond physics at the dawn of the 21st century, for attosecond pulses in the extreme ultraviolet (XUV) spectral region [18]. Most recently, harmonics in the soft x-ray (SXR) region have been reported at a number of laboratories, but very few have been able to characterize the spectral phase [12–14]. Without the spectral phases, the temporal character of the pulse is unknown and any claim of an attosecond pulse is just a guess [19,20].

\*Corresponding author: [cdlin@phys.ksu.edu](mailto:cdlin@phys.ksu.edu)

While attosecond pulses in the SXR regime were first reported in the HHG process, the conversion efficiency is quite small. Typically, it is less than  $10^{-6}$  for HHG, but for XFELs, the efficiency is  $10^{-3}$  of the input energy. While future laser technology might be found to significantly enhance the pulse energy, today it appears that XFELs are more promising for generating intense attosecond x-ray pulses for pump-probe applications [15]. Already, attosecond pulses with central energies near 900 and 540 eV have been reported [15], with pulse energy of the order of  $10 \mu\text{J}$ , with pulse durations around 250 and 450 as, respectively. To reach such conclusions, the phase of the pulses (or the electric field in the time domain) have been characterized by the method reported in [16].

The temporal profiles of isolated attosecond pulses (IAPs) are commonly determined using the “attosecond streaking camera” technique [21–26]. In this method, photoelectron momentum spectra are obtained by the combined field of the IAP and an infrared (IR) laser. At time  $t$ , the IAP releases an electron to the continuum that will gain an additional momentum  $-e\mathbf{A}(t)$  from the IR field, where  $\mathbf{A}(t)$  is the vector potential of the IR at the time of ionization. By changing the time delay between the IAP and the IR, the photoelectron momentum spectra would modulate with the optical period of the IR. For IAPs from the HHG processes, typically linear streaking is employed, where both the IAP and the IR are linearly polarized along the same direction and photoelectron momentum spectra are analyzed only along the the polarization  $x$  direction. By varying the time delay between the two pulses, the resulting two-dimensional streaking spectra (or spectrogram)  $S(p_x, \tau)$  are used to retrieve the temporal electric field of the IAP. Experimentally, at each time delay, the streaking spectra are collected from many shots to obtain good statistics. Good streaking spectra rely on a stable laser system during the time interval where the spectrogram is taken. Different retrieval algorithms have been employed to obtain the temporal dependence of the IAPs from the streaking spectra.

The same “streaking camera” idea was also used for the characterization of IAPs generated at XFEL facilities, with one major difference [16,17] that a spectrogram is not available. In XFELs, each x-ray burst is generated based on the principle of self-amplification of spontaneous emission (SASE). The stochastic nature of SASE results in strong shot-to-shot variations in the temporal profile. Fortunately, the IAPs from the XFELs have sufficient pulse energy to allow single-shot measurements of streaked photoelectron distributions. Earlier efforts for retrieving attosecond pulses from XFELs using linear streaking have been reported in [27–29].

To characterize the IAP in the time domain for each single shot, it has been proposed to modify the “streaking” IR field from linear to a circularly polarized IR field [17]. The simplest geometry is to choose the circularly polarized plane of the IR to be perpendicular to the propagation direction ( $z$  axis) of the IAP. In such a geometry, the photoelectron momentum distribution can be expressed as  $S(p_x, p_y, p_z)$ . A two-dimensional (2D) cut of the momentum spectra  $S(p_x, p_y)$  at  $p_z = 0$  or the two-dimensional spectra obtained by integrating over  $p_z$  [as used in velocity mapping imaging (VMI) spectrometers where the distributions are projected onto a 2D plane] can be analyzed to retrieve the temporal character  $E(t)$  of the IAP.

Depending on the relative phase between the IAP and the circularly polarized IR fields, the 2D spectra  $S(p_x, p_y)$  would rotate on the  $x$ - $y$  plane where the  $x$  axis is the polarization direction of the IAP. Such momentum spectra are called angular streaking spectra. In Li *et al.* [16], using the so-called von Neumann basis, an algorithm has been developed to reconstruct the time-domain IAP and this method was used to obtain the first attosecond pulses from XFELs, reported in Duris *et al.* [15].

The basic idea of the retrieval of  $\mathbf{E}(t)$  of the IAP from  $S(p_x, p_y)$  for each single shot is similar to the retrieval of  $E(t)$  from  $S(p_z, \tau)$  used for attosecond pulses from high-order-harmonic generation, where  $\tau$  is the time delay between the attosecond pulse and the streaking IR field. In both cases, the data are two-dimensional functions, while the unknown  $E(t)$  is one dimensional. While the formal structure of the mathematics is similar, the accuracy and the convergence of the retrieved results are not necessarily the same since the accuracy would depend on the degree of linear independency of the two-dimensional data function.

In this work, we modified the phase retrieval of broadband pulses (PROBP) algorithm [20] used previously for retrieving  $E(t)$  from  $S(p_z, \tau)$  to retrieve  $E(t)$  from  $S(p_x, p_y)$  for each single shot. Since this method is applied to angular streaking, we will call the method PROBP-AS. We compare our retrieved results with the ones from Li *et al.* [16] to show the relative accuracy. Note that the basic idea is very similar in the two methods, except in the computational parametric fitting. Since a typical XFEL experiment will collect a large number of shots, the computing time for each single shot is an important factor for the usefulness of the method, especially when high-repetition MHz rate sources become available.

The theoretical method for our retrieval method is briefly discussed in Sec. II, where we also define how the IAP and IR fields are specified. The results are presented and discussed in Sec. III. A short summary and future applications are given in Sec. IV. Atomic units are used in this article, unless otherwise stated.

## II. STREAKING THEORY AND RETRIEVAL METHOD

To retrieve attosecond pulses from the experimental streaking spectra, a theoretical model to calculate the photoelectron momentum spectra by a given external electromagnetic field is needed. So far, the common method is the so-called strong field approximation (SFA) [19–21]. In SFA, the probability or spectrum  $S(\mathbf{p})$  of an electron ionized from an atom by an external field  $\mathbf{E}(t)$  and that emerges with momentum  $\mathbf{p}$  is given by

$$S(\mathbf{p}) = |\eta(\mathbf{p})|^2 = \left| -i \int dt \{ \mathbf{E}(t) \cdot \mathbf{d}[\mathbf{p} + \mathbf{A}(t)] \} \times \exp \left( -i \int_t^{+\infty} dt_1 \{ [\mathbf{p} + \mathbf{A}(t_1)]^2 / 2 + I_p \} \right) \right|^2. \quad (1)$$

Here,  $\eta(\mathbf{p})$  is the complex probability amplitude for finding an electron with momentum  $\mathbf{p}$ ,  $\mathbf{E}(t)$  is the soft x-ray (SXR) field,  $\mathbf{A}$  is the vector potential of the infrared (IR) field,  $\tau$  is the time delay between the two, and  $I_p$  is the ionization

energy of the target. In this model, the SXR is responsible for the ejection of the electron from the atom, with transition dipole  $\mathbf{d}$  between the ground state and a continuum state with momentum  $\mathbf{p}$ . In this article, the target atom is Ne. Using an SXR pulse with photon energy close to 900 eV, ionization will occur primarily from the  $K$ -shell  $1s$  orbital. In this case, one can approximate  $\mathbf{d}(\mathbf{p}) = \frac{\mathbf{p}}{(\mathbf{p}^2 - 2I_p)^3}$ , which has been checked to agree well with more advanced calculation as long as the continuum electron is not very close to the  $K$ -shell threshold. Since the SXR ionizes the atom in the presence of the IR laser, the photoelectron acquires a phase (or action) as given by the exponential term in Eq. (1). Here,  $\mathbf{A} = -\int_{-\infty}^t \mathbf{E}_{\text{IR}}(t_1) dt_1$  is the vector potential of the streaking IR laser. We chose the polarization direction of the SXR to be along the  $x$  axis and propagating along the  $z$  axis. The IR is circularly polarized on the  $x$ - $y$  plane, which can be expressed as

$$\mathbf{E}_{\text{IR}} = \mathbf{e}_x f(t) \cos[\omega(t - \tau)] + \mathbf{e}_y f(t) \sin[\omega(t - \tau)], \quad (2)$$

where  $\tau$  is the time delay between the two fields, and  $f(t)$  is the envelope of IR.

For a given set of  $\mathbf{E}$ ,  $\mathbf{E}_{\text{IR}}$  (or  $\mathbf{A}$ ) and time delay  $\tau$ , Eq. (1) can be used to calculate photoelectron spectra with momentum components  $(p_x, p_y, p_z)$ . Note that Eq. (1) is based on the SFA model, which is an approximate theory for calculating the 3D electron spectra. In each single-shot experiment, in general, we do not know  $\mathbf{E}$ ,  $\mathbf{E}_{\text{IR}}$  and time delay  $\tau$ . Thus, the goal is to extract these parameters from the measured 3D (or 2D) electron momentum distributions.

In principle, in any streaking experiment, one can measure the photoelectron spectra by the SXR pulse alone. Since photoionization cross sections from the  $K$  shell are quite easy to calculate, such measurement is often carried out from which the amplitude of the attosecond pulse in the spectral domain  $U(\Omega)$  is easily obtained. If this is the case, then one only needs to retrieve the spectral domain phase  $\Phi(\Omega)$ , from which the electric field of the SXR is obtained by a Fourier transformation. In Duris *et al.* [15], however, the spectral amplitudes were measured in separate experiments. Since we are to apply the retrieval method to this experiment, in this article, the  $U(\Omega)$  will be treated as unknown. We remark that if  $U(\Omega)$  is known, the retrieval will be faster and the result will be more accurate since there are fewer parameters to fit.

Thus, to retrieve attosecond pulses for the single shots in Duris *et al.* [15], we need to retrieve the three unknown functions:  $U(\Omega)$ ,  $\Phi(\Omega)$ , and  $f(t)$ , together with the time delay  $\tau$ . For the three functions, we expand each in terms of the B-spline basis,

$$\begin{aligned} U(\Omega) &= \sum_i^{N1} c_i B_i^{k_i}(\Omega), \\ \Phi(\Omega) &= \sum_j^{N2} c_j B_j^{k_j}(\Omega), \\ f(t) &= \sum_l^{N3} c_l B_l^{k_l}(\Omega). \end{aligned} \quad (3)$$

For each set of input parameters, we used Eq. (1) to calculate the electron spectra  $S(p_x, p_y, 0)$ , i.e., we set  $p_z = 0$ . This

2D electron momentum distribution at each iteration step,  $S_{\text{output}}(p_x, p_y)$ , is then compared to the experimental input data,  $S_{\text{input}}(p_x, p_y)$ . The fitness function  $E_f$  is defined by

$$E_f = \sum_{i,j} \min[S_{\text{input}}(i, j), S_{\text{output}}(i, j)]. \quad (4)$$

Note that the theoretical and experimental data are both renormalized to one such that they have the same total yields. The fitness is defined as the overlap of the simulated and experimental data. Here,  $\min(a, b)$  is defined as the smaller value of  $a$  and  $b$ . If the input and the reconstructed functions are exactly the same, the fitness function is equal to 1. With some guessed parameters of these unknown functions, the constructed attosecond and IR are used in Eq. (1) to obtain the electron momentum spectrum  $S(\mathbf{p})$ . By comparing the resulting spectrum with the experiment, a genetic algorithm (GA) is used to select the new guesses for the next iteration (also called generation in GA). The iterative process is terminated after some preselected merit is reached or after a few thousands of iterations.

The efficiency of the GA depends sensitively on the choice of B-spline function parameters, the order  $k$ , and the number of B-spline functions  $n$ . Experimenting on the choice of the input parameters for the GA is necessary. Our strategy is first to run over different combinations of  $(n, k)$  for a few generations (about 200 in this work) and pick the basis set with the fastest change in the fitness function. Based on our observations, running  $k$  from 4 to 8 and  $n$  from 5 to 8 would often guide us to select the best  $n$  and  $k$  for our cases. In the optimization, once we get the best B-spline parameters for IR in the first retrieval calculation, we use these sets of parameters and do not scan them in the remaining retrieval calculations to save time. Details of the GA and B-spline functions can be found in our previous publications [19,20,30,31].

### III. RESULTS AND DISCUSSION

#### A. Retrieved results for 188 shots

Using the methods in the previous section, we first took 25 shots of experimental streaking spectra from the LCLS experiments and analyzed each shot individually. The experimental data are taken with a velocity mapping imaging (VMI) spectrometer; thus it is a 2D projection  $S(p_x, p_y)$  of the 3D momentum spectra integrated over  $p_z$ . In our retrieval, we compare such data to the 2D momentum spectra from Eq. (1) at  $p_z = 0$ , i.e.,  $S(p_x, p_y, p_z = 0)$ . We show, in Appendix C, that this approximation makes only a minor difference to the retrieved results, but saves the computing time.

For each single shot, the unknown functions are the spectral amplitude  $U(\Omega)$ , the spectral phase  $\Phi(\Omega)$  of the attosecond pulse, the envelope  $f(t)$  of the circularly polarized IR laser, plus the time delay  $\tau$  between the attosecond pulse and the IR pulse. The wavelength of the IR is 1300 nm. Each of the three unknown functions is expanded in terms of B-spline functions. By setting the carrier envelope phase (CEP) of the IR equal to zero at  $t = 0$ , the circularly polarized light has a maximum electric field in the  $x$  direction. If the retrieved SXR turns out to be transform limited, then  $\tau$  is the true time delay between the two pulses. Zero time delay

TABLE I. The retrieved parameters of single attosecond pulses for 25 single shots from LCLS experiment.

Shot No.	FWHM (as)	Bandwidth (eV)	Peak position (eV)	Ratio to TL
1	157	13.1	904	1.29
2	184	12.9	904	1.48
3	220	8.1	907	1.12
4	225	9.1	905	1.28
5	225	10.2	903	1.43
6	236	7.4	905	1.09
7	237	8.1	908	1.19
8	241	7.4	904	1.11
9	244	7.4	903	1.13
10	244	7.5	902	1.15
11	245	7.2	904	1.20
12	248	7.5	905	1.16
13	249	7.4	906	1.15
14	249	7.6	905	1.19
15	250	7.2	905	1.13
16	251	7.4	904	1.16
17	252	7.4	906	1.17
18	253	7.5	904	1.19
19	260	7.6	903	1.24
20	263	7.5	906	1.23
21	271	7.6	905	1.29
22	271	7.5	904	1.27
23	331	7.9	906	1.63
24	382	7.8	905	1.86
25	398	7.1	902	1.77

would then mean that the SXR and the  $x$  component of the circularly polarized IR pulse both peak at the same time. If the SXR has significant spectral phase  $\Phi(\Omega)$ , then a Taylor series expansion of the spectral phase around the center  $\Omega_0$  of the spectrum would yield an extra time delay from the linear term of the expansion series. This term is added to  $\tau$  in Eq. (2) when we speak about the time delay between the SXR and the IR.

One interesting question about attosecond pulses generated by XFELs is how each shot differs. Since each pulse is generated stochastically, one may expect that each shot differs from the other without any recognizable pattern. To demonstrate this behavior, in Table I we list the pulse duration (FWHM), the bandwidth, and the peak energy position, as well as the deviation of the pulse duration from a transform-limited one, for a set of 25 shots. One can see that a fair fraction of the shots has duration near 250 as, bandwidth near 7.5 eV, and peak position around 905 eV. The pulse duration typically is only, at most, about 20% from being transform limited. On the other hand, in a few cases, the pulse duration can be as short as 160 as or as long as 400 as. The bandwidth could be as broad as 13 eV, although the peak position is always within a few eV from the most probable one at 905 eV. We have not found pulse duration more than twice the transform-limited one. For further comments on this statement, see Sec. III C.

It is well understood that a complete characterization of a pulse requires knowing both the amplitude and phase in the time domain or in the energy domain, respectively. Al-

ternately, one can show the intensity in the time domain and spectral domain together. In Table I, we order these shots according to the FWHM duration, starting with No. 1 being the shortest. In Fig. 1, we show the time-domain intensities, while the intensities in the energy domain are shown in Fig. 2. From Fig. 1, as the FWHM duration increases (increasing shot number), the pedestals away from the peaks tend to show larger substructures. Such substructures do not appear in the spectral intensity, as shown in Fig. 2. These two sets of figures follow the general trend that a shorter pulse in the time domain is accompanied by a broader bandwidth in the energy domain. From Table I, the retrieved pulses follow this prediction, but small deviations do occur owing to the presence of chirps in the spectral phase. In the meanwhile, while the center of the spectral intensity is clustered around 905 eV, deviations of 2–3 eV are observed. Table I also shows that the bandwidth of these 25 shots is about 7.5 eV, but there are shots where the bandwidth is near 13.0 eV. The last column of Table I shows that the typical deviation of each shot from being a transform-limited pulse is within about 20%, but larger deviation also occurs. These results for the 25 pulses are expected to represent typical variations of different single-shot attosecond pulses generated at XFEL facilities. It also means that an efficient pulse characterization algorithm is needed in order to use such attosecond pulses for applications.

We next examine if the pulse duration and bandwidth distributions show some pattern. First, Figs. 3(a)–3(d) compare the pulse duration and bandwidth distributions of two different sets of 25 shots. While the most probable pulse durations and bandwidths are about the same for the two sets, the distributions outside of the most probable region are different. Figures 3(e) and 3(f) show the results for the 188 shots that we have analyzed. The number of pulses that have durations longer than 250 as drops monotonically, but the bandwidth distribution tends to cluster around the most probable value of 7.5 eV. While it is fair to say that more than half of the 188 shots have pulse durations within  $250 \pm 50$  as, each shot has to be reconstructed individually. Thus, an efficient reconstruction algorithm for each shot from the measured streaking spectra is highly desirable.

Similarly, in Fig. 4, we compare the distribution of the peak energy positions and the time delays between the SXR and IR pulses for two sets of 25 shots each [Figs. 4(a)–4(d)] and for the total 188 shots [Figs. 4(e) and 4(f)]. The half width of the peak position is about 2 eV centered at 905 eV. Interestingly, the retrieved time delays are always quite small, mostly within only about 20–40 as. This result seems surprising. It turns out that these 188 shots were not selected randomly, but were prefiltered. We will come back to address this observation in Sec. III B.

In Fig. 5(a), we display the degree of deviation of each retrieved pulse duration from a transform-limited (TL) one. The majority of the shots have durations less than 50% longer than the TL one. Figure 5(b) shows the overlap integral between the experimental 2D streaking spectra and the one generated using the SFA model with the optimized pulse for each shot. The typical overlap is from 0.942 to 0.945. Ideally, this overlap is 1.0, but it should not be since the streaking spectra were calculated based on the SFA; see Eq. (1). The SFA is not an exact theory for describing the ionization spectra by a

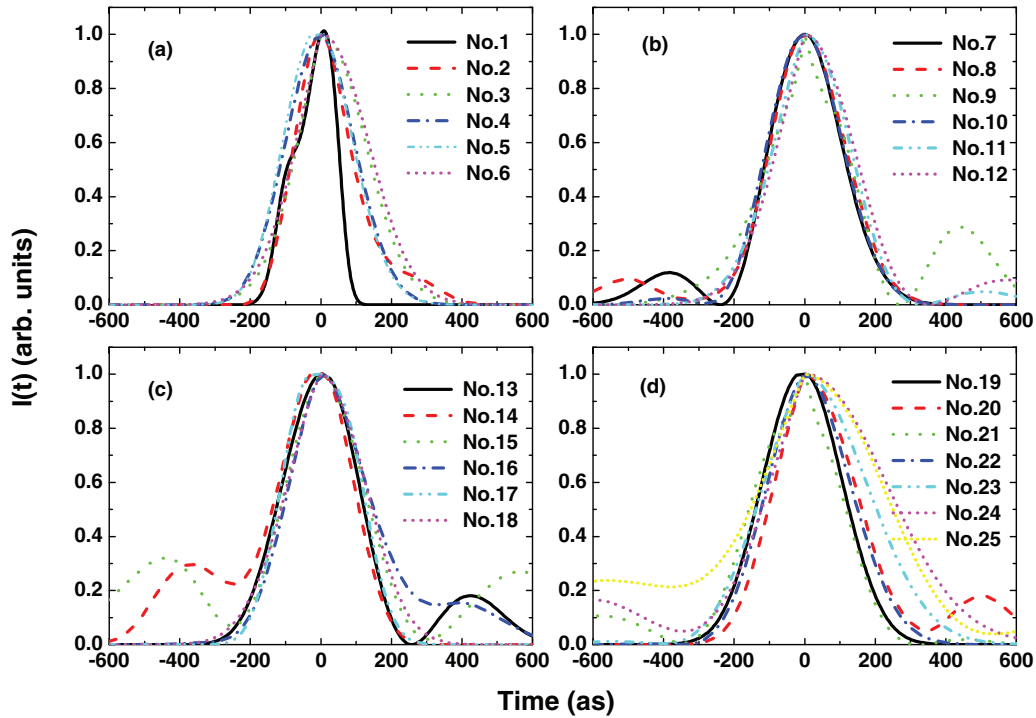


FIG. 1. Reconstructed temporal intensities  $I(t)$  for 25 experimental attosecond pulse shots, ordered by FWHM duration from the shortest to the longest. The pulse energy at the peak has been normalized to 1. Pulses that have longer durations are those that exhibit more pronounced substructures away from the main peak.

two-color pulse. Additionally, experimental data always have intrinsic errors. In our optimization, if the overlap is less than 0.940, we would run GA another thousand steps to check if convergence has been achieved.

### B. Time delays between the two pulses

The IR laser is stabilized with respect to the rf which drives the accelerator. However, there are still shot-to-shot fluctuations in the arrival time of the x-ray pulse relative to

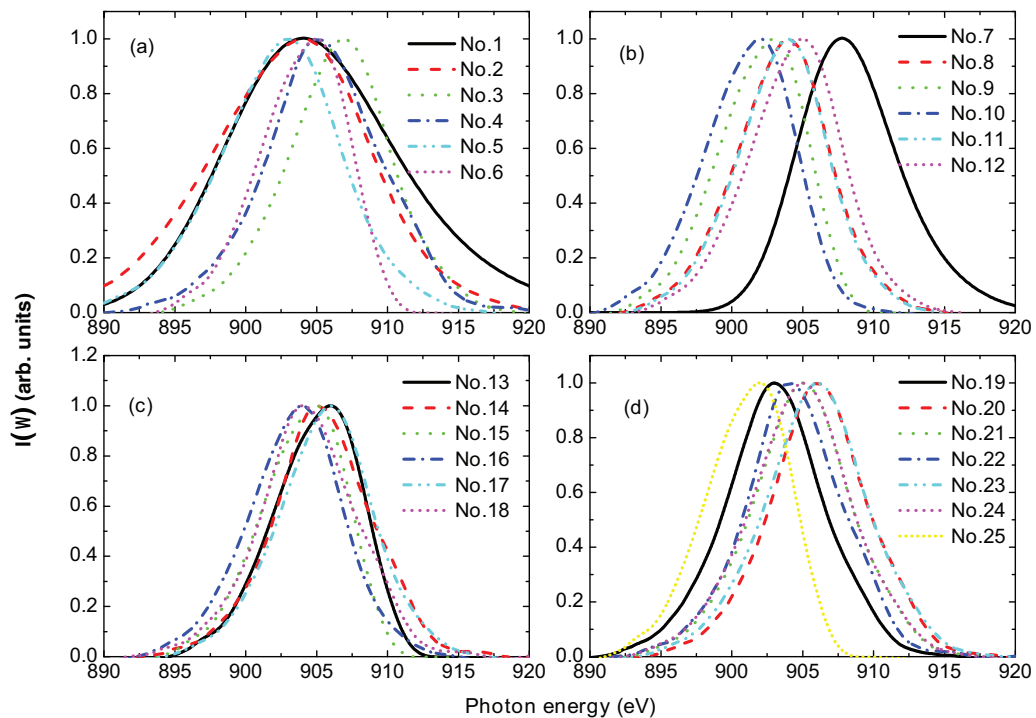


FIG. 2. Reconstructed spectra intensity  $|E(\Omega)|^2$  for the same 25 experimental shots shown in Fig. 1. Each pulse is labeled by its shot number as in Table I. The intensity at the peak for each shot has been normalized to 1. The color scheme is the same as that in Fig. 1.

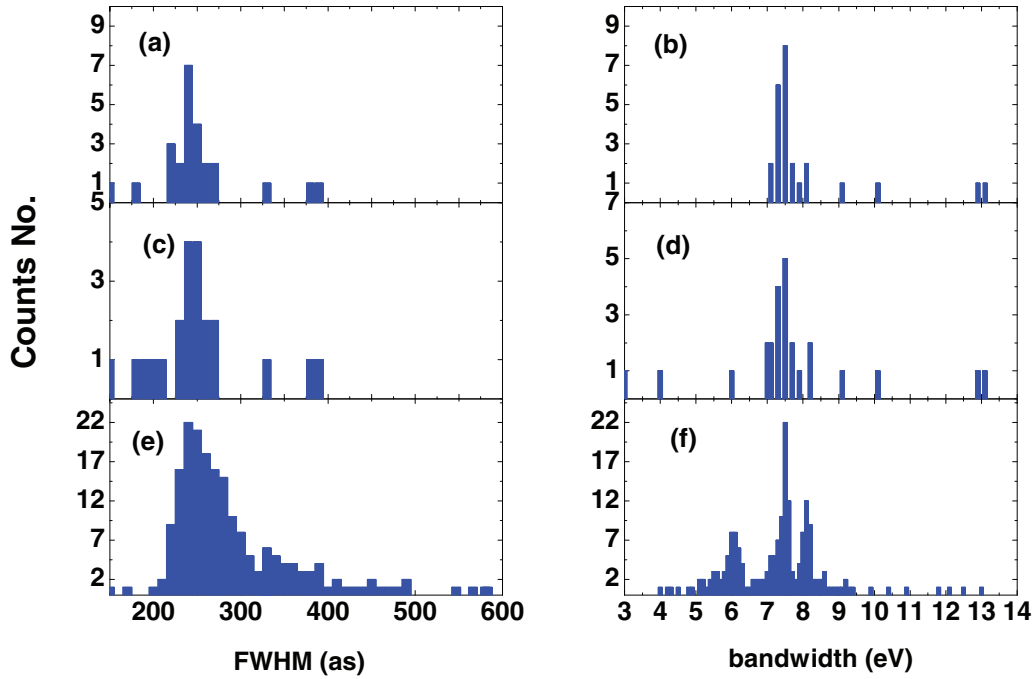


FIG. 3. FWHM pulse duration and bandwidth distributions for three sets of pulses. (a),(b) and (c),(d): two sets of 25 different shots; (e),(f) one set of 188 shots. On the left column, each bar has width of 10 as, while on the right column, each bar has width of 0.1 eV.

this rf signal. As the result, the relative time delay between the x-ray and IR laser field for each shot is to be extracted from the measured 2D electron spectra as well. In the experiment of [15], the duration of each SXR shot is of the order of a few hundred attoseconds, which is much shorter than the about

100 fs multicycle 1300 nm streaking laser; the time delay  $\tau$  between the two pulses can be determined only up to the 4.4 fs optical period of the 1300 nm laser. (For shorter few-cycle IR fields, the amplitude of each cycle is different; then the true time delay can be retrieved using our method [20].)

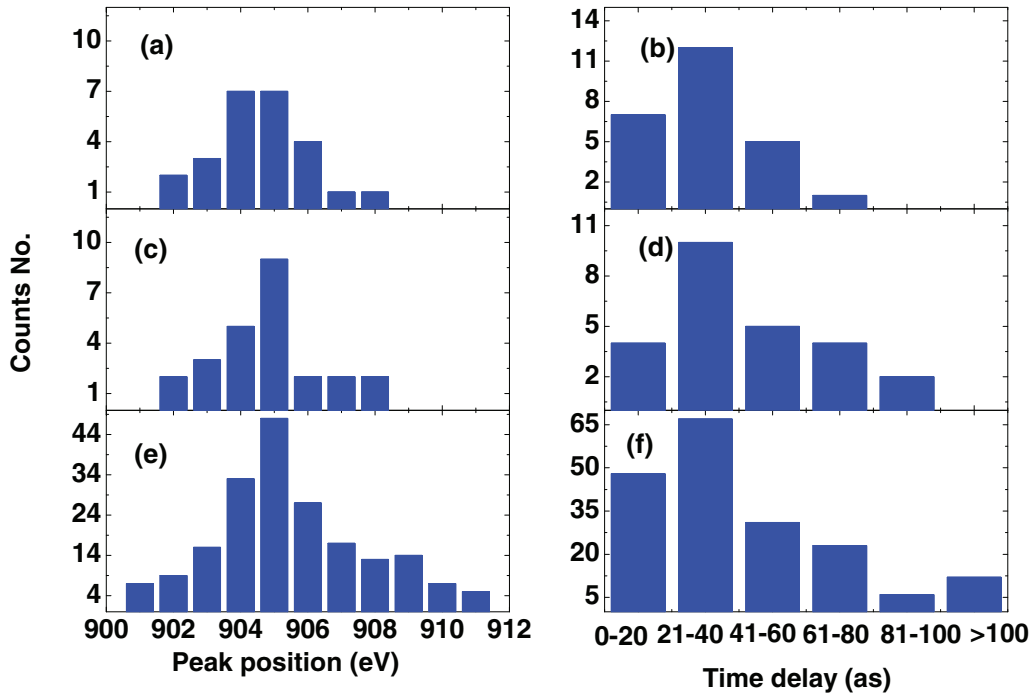


FIG. 4. Peak position and time delay distributions from (a),(b) and (c),(d) the same two sets of 25 shots, and (e),(f) one set of 188 shots. The data are the same as those in Fig. 3. On the left column, each bar has width of 1 eV, while on the right column, each bar has width of 20 as.

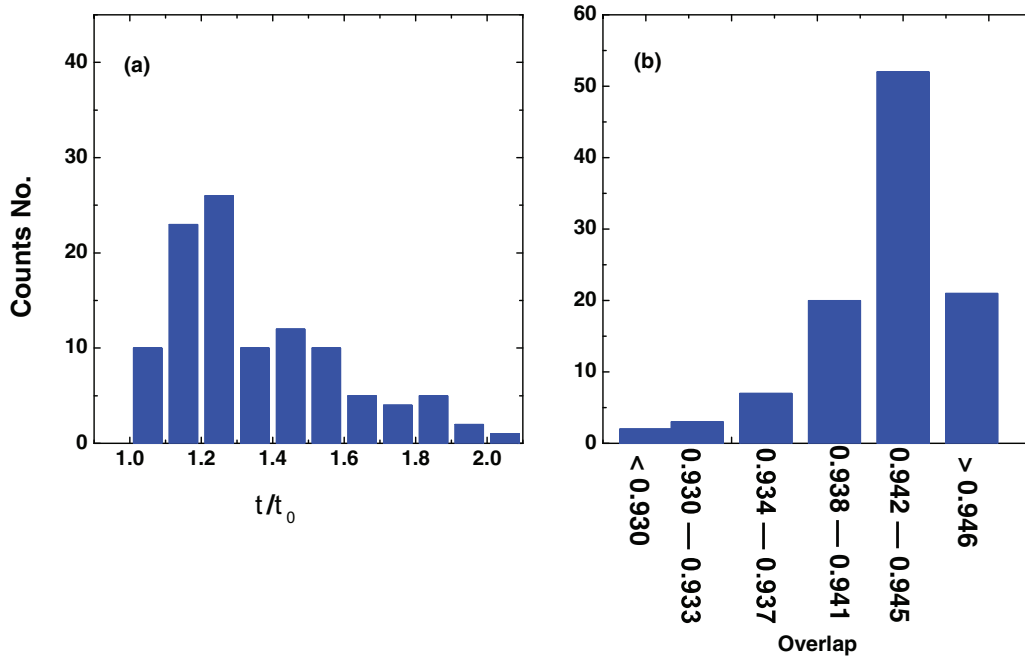


FIG. 5. (a) The distribution of pulse durations  $\tau/\tau_0$  for the 105 shots retrieved. (b) The overlap integral of the experimental 2D electron spectra with the one calculated using the retrieved pulse. Here,  $\tau_0$  is the duration of a transform-limited pulse.

Before presenting the retrieved time delays, let us first examine how the SFA model predicts the 2D  $S(p_x, p_y)$  electron spectra versus the time delay. For this purpose, we consider a transform-limited attosecond pulse which has central energy at 905 eV, bandwidth of 7.5 eV, and the target is Ne. In the absence of the IR laser, the photoelectron spectra are shown

in Fig. 6(f). The 2D electron spectra has reflection symmetry with respect to the  $p_x$  and  $p_y$  axis. Clearly, the center of the electron spectra is located at  $(p_x, p_y) = (0.0, 0.0)$ . In the presence of the IR laser, the symmetry is modified since the photoelectron, once lifted from the  $K$  shell, will receive an additional momentum  $-e\mathbf{A}(\tau)$  from the IR field. For  $\tau = 0$ ,

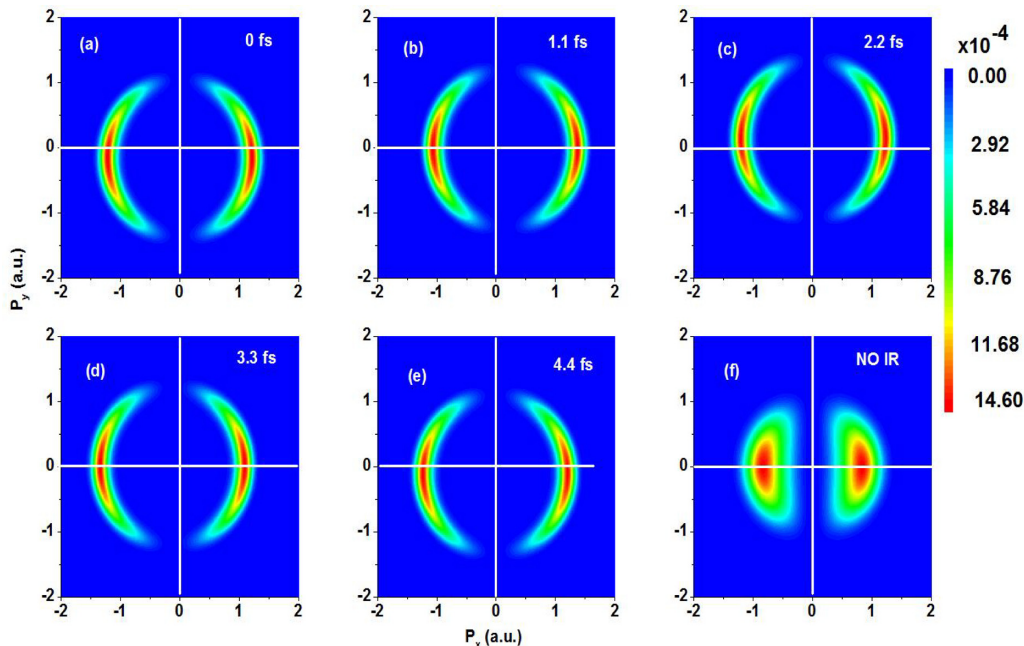


FIG. 6. SFA calculations showing how the center of the streaking spectra shifts with the time delay within one optical cycle of the IR. The electron spectra  $S(p_x, p_y)$  are generated with a transform-limited attosecond pulse with central energy at 905 eV, bandwidth of 7.5 eV, and pulse duration of 210 fs (FWHM). The IR is 1300 nm with FWHM duration of 80 fs, the intensity is  $10^{12}$  W cm $^{-2}$ , and the target is the Ne 1s orbital. Without the IR, the center of the spectra is located at  $(p_x, p_y) = (0.0, 0.0)$ ; see (f). In the presence of the IR, the centers for (a)–(e) at  $\tau = 0.0, 1.1, 2.2, 3.3,$  and  $4.4$  fs are shifted to  $(0, -0.19), (0.19, 0.0), (0.0, 0.19), (-0.19, 0.0),$  and  $(0.0, -0.19)$ , respectively.



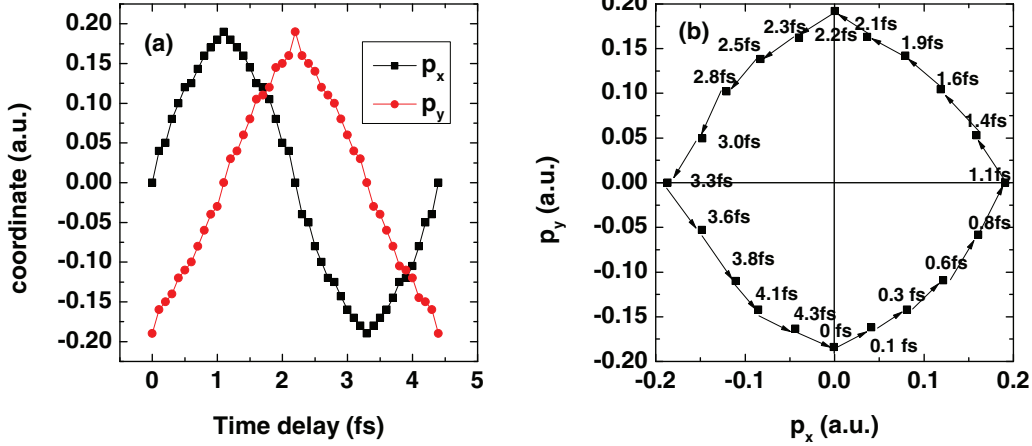


FIG. 7. (a) The coordinates of the center of each momentum distribution vs the time delay for fixed SXR and IR pulses, calculated using the SFA. The red circles are for  $p_y$ , and the black squares are for  $p_x$ . (b) Parametric plot of the position of the center of the streaked electron spectra on the  $(p_x, p_y)$  plane vs the time delay between the SXR and IR. The center (0,0) is for the case in the absence of the IR. Parameters for the SXR and the IR are the same as in Fig. 6.

with the IR used, this vector potential is  $-0.19$  a.u. along the  $y$  axis, such that the center of the 2D spectra will be shifted to  $(p_x, p_y) = (0, -0.19)$ . If  $\tau = 1.1$  fs, i.e., at a quarter optical cycle later, the center will be located at  $(p_x, p_y) = (0.19, 0.0)$ . Likewise, at  $\tau = 2.2$  fs, the center is at  $(0.0, 0.19)$ , and at  $\tau = 3.3$  fs, the center is at  $(-0.19, 0.0)$ . As the time delay reaches one full optical cycle, the center returns to  $(p_x, p_y) = (0, -0.19)$ , which is the same as for  $\tau = 0$ . These streaking spectra are shown in Figs. 6(a)–6(e). In fact, based on the SFA theory, we can calculate the peak position of the streaking spectra on the left (negative  $p_x$ ) and on the right (positive  $p_x$ ), respectively, from which the center of the streaked 2D electron spectra can be calculated. In Fig. 7(a), we show the  $p_x$  and  $p_y$  points of these centers for each time delay, and in Fig. 7(b), the  $(p_x, p_y)$  points trace a symmetric loop which is close to, but not, a circle. Deviation from a perfect circle occurs since electrons are emitted over the pulse duration (about 250 as) of the SXR.

It is interesting to point out that at the symmetry points of Fig. 7(b), for time delays at 0.0, 1.1, 2.2, and 3.3 fs, the 2D electron spectra are essentially the replica of the spectra at  $\tau = 0$ . By shifting each of the streaking spectra such that the center coincides with the one for  $\tau = 0$ , we found that the shifted spectra have very good overlap with the spectra from  $\tau = 0$ , with a deviation from 1.0 by less than 0.2%.

In a typical pump-probe experiment, to claim temporal resolution of an attosecond pulse, the uncertainty of the time delay in a single-shot experiment should be added to the duration of the attosecond pulse as well. In Fig. 4, we have reported time delays from the 188 shots that lie mostly under 60 as, with a few closer to 100 as. To check how accurately the time delay can be retrieved from our algorithm, we use SFA to generate the streaking spectra with known SXR and IR lasers, and known time delays. We then use our algorithm to retrieve the input parameters from the calculated 2D momentum spectra, but now only focusing on the retrieved time delay. The results are displayed in Table II. Clearly, the retrieved time delay shown in the second column for each shot differs from the input time delay by typically only a few tens

of attoseconds. These results show that the present retrieval method is capable of retrieving a time delay of the order of about 100 as using the 1300 nm IR laser as the streaking field. In this respect, the time delays reported in Fig. 4(f) for the 188 shots from the experimental data [15] are not taken to be significant since they all fall within 100 as. This has to do with the fact that these 188 shots have been prefiltered. It shows that the filtering method used by the experimentalists is capable of differentiating time delays within about 100 as.

### C. Comparison with other retrieval method

Single-shot attosecond pulses from the LCLS experiment reported in Duris *et al.* [15] have been reconstructed using the retrieval method given in the paper by Li *et al.* [16]. Comparing their method with ours, the starting point is the same. Both methods use the strong field approximation to obtain the angular streaking spectra. The main difference between our PROBP-AS and theirs is the retrieval algorithm. In the approach of Li *et al.* [16], they expand

$$\vec{E}(t) \cdot \vec{d}(t) = \sum_n c_n \alpha_n. \quad (5)$$

TABLE II. Investigation of the accuracy of the retrieved time delays. The SFA model is used to calculate  $S(p_x, p_y)$  with different input time delays. The retrieved time delays from the calculated  $S(p_x, p_y)$  are then compared to the input ones. The results show that error from the retrieval method is a few tens of attoseconds.

Input time delay (fs)	Output time delay (as)
180	154
360	444
550	633
730	711
1650	1713
2880	2819
4200	4259

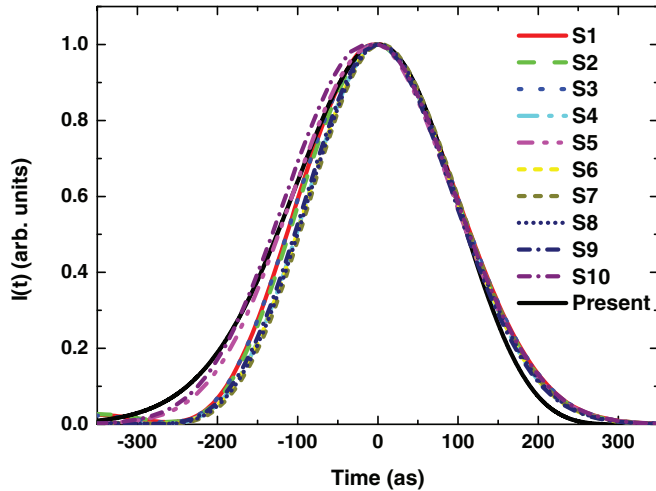


FIG. 8. Comparison of the retrieved temporal intensity distributions from 10 different initial conditions obtained in Ref. [16], with the optimized one using the present PROBP-AS method. Many “good” pulses from Ref. [16] can be found to be very close to each other and agree with the one retrieved using the present method, including the magnitude of the overlap between the experimental streaking spectra and the one generated (using SFA) with the retrieved pulse.

Here,  $\alpha_n(t)$  is the von Neumann function which is a joint time-frequency basis,

$$\alpha_{ij}(t) = \left( \frac{1}{2\alpha\pi} \right)^{\frac{1}{4}} \exp \left[ -\frac{(t-t_j)^2}{4} - it\omega_j \right], \quad (6)$$

where  $\alpha$  is a constant specified by the range and size of the von Neumann lattice, and the lattice points  $(t_i, \omega_j)$  are grid points in time and frequency. For each shot, a set of  $c_n$  is first guessed to construct the streaking spectra. The calculated streaking spectra are then compared to experiments until the difference squared is smallest. In our PROBP-AS approach, we use B-spline functions to expand the unknown functions instead. The circularly polarized IR field in the experiment of Duris *et al.* has a pulse duration of  $\sim 100$  fs, and thus the IR field is taken as a plane wave. They also set the SXR pulse and the IR to arrive at the same time which is set to  $t = 0$ , or  $\tau = 0$ , but the IR has a relative phase  $\phi$  with respect to the SXR. As described in Sec. II, we parametrize the SXR in the energy domain for both the amplitude and phase. The envelope function of the IR as well as time delay  $\tau$  are also determined from the retrieval.

In [16], the reconstruction starts with 100 random Monte Carlo initial guesses and each guess is run for 100 iterations.

TABLE III. Comparison of the 10 retrieved results from Li *et al.* [16] with the one from the present method. Shown are the FWHM pulse durations and the overlap of the electron momentum distribution for each pulse with the experimental streaking spectra.

	S1	S2	S3	S4	S5	S6	S7	S8	S9	S10	Present
FWHM (as)	245	232	225	247	243	232	242	232	248	244	250
Overlap	0.946	0.940	0.939	0.946	0.943	0.941	0.942	0.941	0.951	0.943	0.945

For each initial guess, the fitness parameter is calculated as

$$\sigma_x = \sqrt{\frac{\sum_j^N \left( x_j - \frac{\sum_i^N I(x_i)x_i}{\sum_i^N I(x_i)} \right)^2 I(x_j)}{\sum_j^N I(x_j)}}, \quad (7)$$

where  $I$  is the laser intensity and  $x$  is the anchored points of time. It is found that the best reconstructed pulse lies close to those that have the largest occurrence of fitness.

Figure 8 shows the temporal profiles of 10 SXR pulses retrieved for a single shot that have the higher occurrence of the same fitness. They all lie close to the single optimized pulse retrieved using the present method. One way to measure the “goodness” is to compare the overlap of the experimental spectra with the one calculated from the retrieved one. As shown in Table III, the highest overlap is 0.95 (S9), which gives a FWHM duration of 248 as. The overlap from our method is 0.945, which has FWHM duration of 250 as. In fact, the 10 pulses shown in Table III have pulse duration within 10% of the optimized one.

In comparing the difference between the two methods, we point out that in [16], the electric field of the SXR pulse in the time domain is directly retrieved using discrete points of von Neumann basis and the results are quite “spiky” versus time if a small number of points is used. To obtain the pulse in the energy domain, the Fourier transformation of the time-domain field was smoothed with a Gaussian filter. This would introduce errors in the spectral domain properties. In [16], the IR field is taken as a plane wave and the time delay was set at zero. Such assumptions would have to be removed if accurate time delays are to be retrieved with the use of a few-cycle IR field. In our PROBP method we used B-spline functions to represent the amplitude and phase of the SXR pulse in the energy domain. The time-domain pulse is obtained directly by Fourier transform. The present method can also retrieve the IR field and the time delay without any modification when such experiments are carried out using few-cycle IR pulses. In addition, if experiments do measure the single-photon ionization spectra by the SXR pulse alone, the spectral amplitude can be determined directly. Such information can be used to check the accuracy of the retrieval method or to remove the need to fit  $U(\Omega)$  in Eq. (3).

While direct comparison of computer running time for each shot has not been done, to obtain the result reported in this article, it normally takes about 20 minutes to get the converged result by running our code on an Intel Xeon E5-2609 CPU single core computer. For shots that have larger chirp, more iterations will be carried out for twice the number of iterations. If the convergence is not good, the overlap tends to be less than 0.93.

#### IV. DISCUSSION AND SUMMARY

In this article, we have extended the PROBP [20,31–34] phase retrieval method for reconstructing the temporal character of attosecond pulses from high-order-harmonic generation to attosecond pulses generated using x-ray free-electron lasers. The latter is unique in that single attosecond pulses are generated stochastically, and thus the traditional streaking method cannot be applied. Instead, using a circularly polarized IR laser as the “streaking” field, two-dimensional (or three-dimensional) photoelectron spectra for each single shot can be used to retrieve the one-dimensional information on the amplitude and phase of each attosecond pulse, either in the time domain or in the energy domain. We used PROBP-AS to denote this modified method for phase retrieval, where AS stands for angular streaking.

We have applied the PROBP-AS method to retrieve 188 single shots from the experimental data reported in Duris *et al.* [15]. Previously, an alternative retrieval method [16] was used. As shown in Sec. III C, we have compared the retrieved results from the two methods and they agree well, except that the PROBP-AS method is able to retrieve the IR pulse as well as the time delay between SXR and IR pulses. We have shown in detail how the attosecond pulse from each shot is different, in the time domain or in the energy domain, for 25 shots. We then demonstrated that the distributions of pulse durations of the 188 shots are clustered around 250 as, with a tail reaching to about 500 as. In the meanwhile, in the energy domain, the most probable peak position is 905 eV and the bandwidth is 7.5 eV. Most of the shots are close to transform limited, with pulse durations within 20% of a TL pulse. This is also in agreement with simulations of the FEL which predict nearly transform-limited pulses. We comment that this is significantly different from the SXR attosecond pulses generated by high-order-harmonic generation in a gas where the bandwidth is several hundreds of electron volts. The spectral phase over this large energy range can become quite large, making accurate phase retrieval more difficult; see Ref. [19].

We also have retrieved the time delay for each shot. Since the streaking IR field is about 100 fs, one can obtain the time delay within one optical cycle, which is 4.4 fs. We have demonstrated that the time delay can be retrieved accurately to a few tens of attoseconds. So we are comfortable in claiming that the time delay accuracy of about one-hundred attoseconds is reasonable. To obtain the actual time delay between the SXR and the IR, a few-cycle IR pulse must be used. The PROBP-AS algorithm can retrieve the IR field as well, and thus the real time delay between the SXR and the IR can also be determined for each shot.

Before closing, it is pertinent to comment that we have tested other factors that can contribute errors to the present retrieval method. They include the use of the strong field approximation in calculating the photoelectron momentum spectra, and the validity of approximating the  $p_z$  integrated 2D electron momentum spectrum with the one at fixed  $p_z = 0$ . These issues are documented in the Appendix. We also have checked the possible error in the retrieved SXR if the IR field is not pure circularly polarized. We found that the effect is small, so it is not presented. Generally speaking, we expect that 10% accuracy of the retrieved pulse duration is reasonable.

In conclusion, we have developed a PROBP-AS retrieval algorithm that allows us to retrieve accurate isolated attosecond pulses generated stochastically from x-ray free-electron lasers. The method is accurate and fast. In the future, if photoelectron spectra by the SXR alone are also measured in the experiment for each shot, the retrieval will be even quicker and the result will be more accurate.

Looking ahead, it is possible to extend the present retrieval method to a double pulse made of two single IAPs that is to be used for attosecond pump-probe experiments. The stochastic nature of each shot would make it essential to characterize each single shot in such experiment, and a very fast algorithm for characterizing each shot is essential for interpreting the experimental data [35].

#### ACKNOWLEDGMENTS

This work was supported by U.S. Department of Energy (DOE), Office of Science, Office of Basic Energy Science (BES), Chemical Sciences, Geosciences and Biosciences Division under Grant No. DE-FG02-86ER13491, by the DOE-BES, Chemical Sciences, Geosciences, and Biosciences Division, by DOE-BES under Contract No. DE-AC02-76SF00515, DOE-BES Accelerator and detector research program Field Work Proposal 100317, and DOE Laboratory Directed Research and Development program at SLAC National Accelerator Laboratory, under contract DE-AC02-76SF00515. Use of the Linac Coherent Light Source (LCLS), SLAC National Accelerator Laboratory, is supported by the U.S. Department of Energy, Office of Science, Office of Basic Energy Sciences under Contract No. DE-AC02-76SF00515.

#### APPENDIX

##### 1. Validity of the SFA model

Our method for calculating the electron spectra is based on the SFA, which does not contain Coulomb interaction between the photoelectron and the ionic core. While the electron spectra are more accurately calculated by solving the time-dependent Schrodinger equation (TDSE), the latter cannot be used for the retrieval since each calculation would take a much longer time. To examine the error introduced from the SFA, we solve the TDSE to obtain the photoelectron spectra and use it as an “experimental” result with known XUV and IR parameters. We then use the PROBP-AS algorithm to see how well the XUV attosecond pulse is retrieved. Figure 9 shows the result for the case where the IAP is a TL pulse. In Fig. 9(a), the retrieved temporal intensity profile shows a longer pulse duration (90 as for the retrieved one compared to 82 as for the input). In Fig. 9(b), the retrieved spectral phase acquires a few subradians instead of the zero phase in the input. In Fig. 9(c), the retrieved spectral bandwidth is a bit narrower than the input one. In Fig. 9(d), the 2D electron spectra  $S(p_x, p_y)$  have been integrated over  $p_x$  or  $p_y$  to get the 1D electron spectra  $D(p_x)$  and  $D(p_y)$ . The resulting  $D(p_x)$  and  $D(p_y)$  from the two calculations are compared. It shows that the photoelectron spectra calculated using SFA with the retrieved pulse is in good agreement with the spectra obtained from TDSE calculations. A similar comparison has been made for the case where the input IAP is chirped. As shown in Fig. 10, the

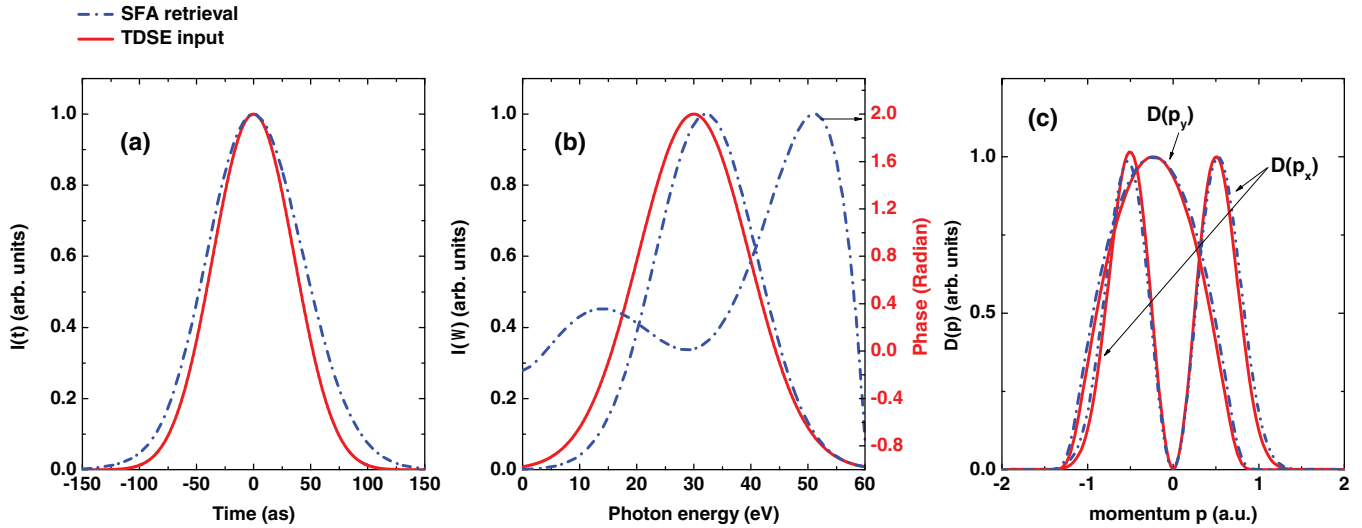


FIG. 9. This figure illustrates the degree of errors for using the SFA to retrieve attosecond pulses. The spectra calculated from solving the TDSE are taken as experimental data, while the SFA is used to retrieve the pulse duration. The input pulse is a TL with zero phase over 11 eV spectral range. (a) The retrieved and the input temporal intensities are compared. The FWHM differs by about 10% (90 as compared to the input one at 82 as.) (b) Comparing the input spectral intensity and phase with the retrieved ones showing errors of subradians away from the center of the spectra. (c) The streaking spectra integrated over  $p_y$  or  $p_x$  from the TDSE and from the retrieved pulse using the SFA are compared. The 2D streaking spectra from TDSE have a 0.955 overlap with the one obtained from the retrieved pulse using the SFA. The calculation was carried out with parameters that are used for laser experiments. The overlap will increase with higher photoelectron peak energy since the SFA becomes a better approximation at higher energy. The two-peak lines are for  $D(p_x)$ , and the one-peak lines are for  $D(p_y)$ .

relative accuracy is not significantly different. Based on these results, we can say that retrieval methods based on SFA do not cause significant errors when the electron has energy at and above 30 eV. Clearly, the Coulomb effect becomes stronger as the electron energy is reduced. Thus, for pulse retrieval, one should avoid using low-energy photoelectrons.

## 2. Comparing details between the two retrieval methods

In Fig. 8, we compare the temporal intensity of the retrieved IAP from the experimental data using our method and compared it to 10 retrieved pulses obtained using the method

of [16]. In Fig. 11, we show that even for the worst retrieved pulse (S3) among the 10 (see Table II), the discrepancy is not that large. On the other hand, it is clear that the best retrieved pulse (S9) does agree well with the one retrieved using the PROBP-AS method. This can be seen clearly in Figs. 11(b) and 11(c), where we compare  $D(p_x)$  and  $D(p_y)$  which is obtained by integrating over  $p_y$  or  $p_x$  for the cases: three pulses S3 and S9 from using the method of [16], and from PROBP-AS. One can see, indeed, that the discrepancy from S3 has a larger error, while the S9 and the one from PROBP-AS both agree with each other.

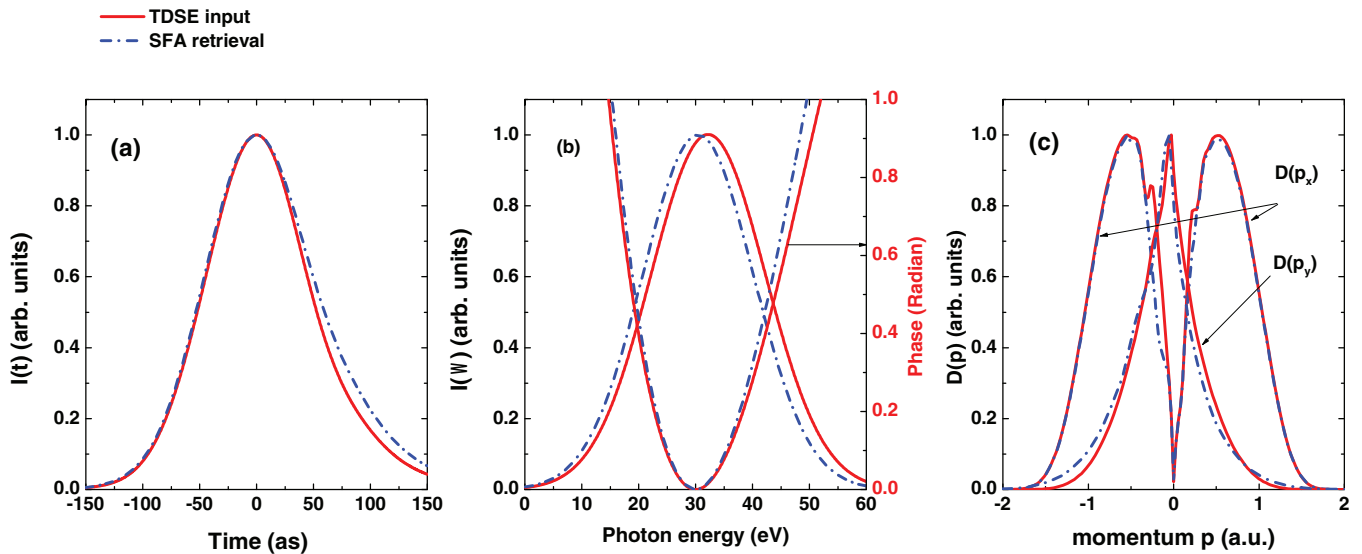


FIG. 10. Same simulation as in Fig. 9, but the input IAP is a chirped pulse. The two-peak lines are for  $D(p_x)$ , and the one-peak lines are for  $D(p_y)$ .

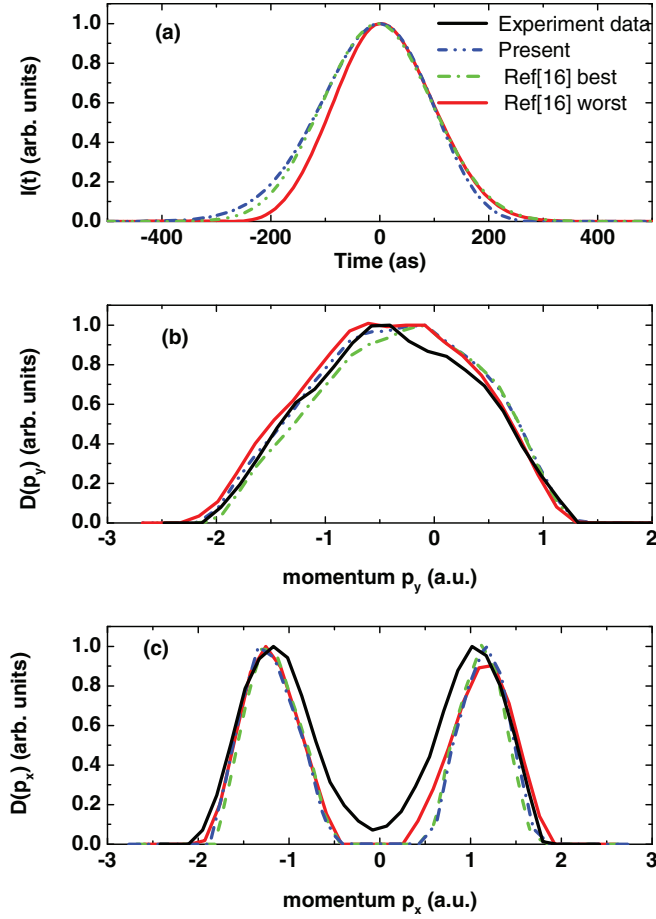


FIG. 11. Consistency check between the present result and those from [16]. (a) Retrieved intensity profile from the present method as compared to the best retrieved one (determined by the overlap of the experimental streaking spectra with the one generated from the retrieved pulse). It shows that even for the “worst” overlap case (S3), the discrepancy is small. (b),(c) Comparing the 1D  $p_y$  and  $p_x$  integrated spectra respectively. On the graphs, even for the one from S3, the discrepancy to experiment is small. These results demonstrate that the pulse retrieved from the present method agrees better with the best retrieved one from [16], but even the results from the worst one from [16] are not bad.

### 3. Validity of comparing $p_z$ -integrated $S(p_x, p_y)$ with $S(p_x, p_y, p_z = 0)$ spectra

In the experiment of Duris *et al.* [15], the 2D electron momentum spectra are obtained from the 3D spectra integrated over  $p_z$ . Rigorously speaking, to retrieve the attosecond pulses, at each iteration, the 3D electron spectra have to be calculated from the SFA and then integrated over  $p_z$  such that same parameters are compared in the retrieval process. We have tested that this integration step can be omitted by just setting  $p_z = 0$ .

Here we provide a mathematical derivation to prove the validity of the  $p_z = 0$  approximation. Starting with Eq. (1),

$$\eta(\mathbf{p}) = -i \int dt \{\mathbf{E}(t) \cdot \mathbf{d}[\mathbf{p} + \mathbf{A}(t)]\} \times \exp\left(-i \int_t^{+\infty} dt_1 \left\{ \frac{[\mathbf{p} + \mathbf{A}(t_1)]^2}{2} + I_p \right\}\right), \quad (\text{A1})$$

we evaluate the integral over  $t$  using a saddle-point approximation, as Lewenstein *et al.* and many other works did in Refs. [36–41]. Let

$$g = -i \int_t^{\infty} dt_1 \left\{ \frac{[\mathbf{p} + \mathbf{A}(t_1)]^2}{2} + I_p \right\}, \quad (\text{A2})$$

where we have  $\frac{dg}{dt} = -i \left\{ \frac{[\mathbf{p} + \mathbf{A}(t)]^2}{2} + I_p \right\}$ ,  $\frac{d^2g}{dt^2}|_{t=t_s} = i[\mathbf{p} + \mathbf{A}(t_s)] \cdot \mathbf{E}_{IR}(t_s)$ . Then,

$$\eta(\mathbf{p}) = -i \frac{\mathbf{E}(t_s) \cdot \mathbf{d}[\mathbf{p} + \mathbf{A}(t_s)]}{\sqrt{i[\mathbf{p} + \mathbf{A}(t_s)] \cdot \mathbf{E}_{IR}(t_s)}} \times \exp\left(-i \int_{t_s}^{\infty} dt_1 \left\{ \frac{[\mathbf{p} + \mathbf{A}(t_1)]^2}{2} + I_p \right\}\right). \quad (\text{A3})$$

For the electron ionized from the 1s orbital of the atom, the transition dipole moment can be approximated by a Gaussian form,  $d(\mathbf{p}) = i \left(\frac{1}{\pi\alpha}\right)^{3/4} \frac{\mathbf{p}}{\alpha} \exp\left(-\frac{p^2}{2\alpha}\right)$ , with  $\alpha = 0.8I_p$ . Then we have

$$S(\mathbf{p}) = |\eta(\mathbf{p})|^2 \approx \frac{\mathbf{E}^2(t_s)}{[\mathbf{p} + \mathbf{A}(t_s)] \cdot \mathbf{E}_{IR}(t_s)} \left(\frac{1}{\pi\alpha}\right)^{3/2} \frac{(p_x + A_x)^2}{\alpha^2} \times \exp\left[-\frac{(p_x + A_x)^2 + (p_y + A_y)^2 + p_z^2}{\alpha}\right]. \quad (\text{A4})$$

Recall that the IR is on the  $XY$  plane, and SXR is polarized along the  $x$  axis. Integration over  $p_z$  gives

$$\begin{aligned} \int S(\mathbf{p}) dp_z &= \int |\eta(\mathbf{p})|^2 dp_z \\ &\approx \frac{\mathbf{E}^2(t_s)}{[\mathbf{p} + \mathbf{A}(t_s)] \cdot \mathbf{E}_{IR}(t_s)} \left(\frac{1}{\pi\alpha}\right)^{3/2} \frac{(p_x + A_x)^2}{\alpha^2} \\ &\times \exp\left[-\frac{(p_x + A_x)^2 + (p_y + A_y)^2}{\alpha}\right] \\ &\times \int \exp\left(-\frac{p_z^2}{\alpha}\right) dp_z \\ &= \frac{\mathbf{E}^2(t_s)}{[\mathbf{p} + \mathbf{A}(t_s)] \cdot \mathbf{E}_{IR}(t_s)} \left(\frac{1}{\pi\alpha}\right)^{3/2} \frac{(p_x + A_x)^2}{\alpha^2} \\ &\times \exp\left[-\frac{(p_x + A_x)^2 + (p_y + A_y)^2}{\alpha}\right] \sqrt{\alpha\pi} \\ &= \sqrt{\alpha\pi} S(p_x, p_y, p_z = 0). \end{aligned} \quad (\text{A5})$$

This shows that integration over  $p_z$  gives an overall normalization, and we can save computing time significantly without

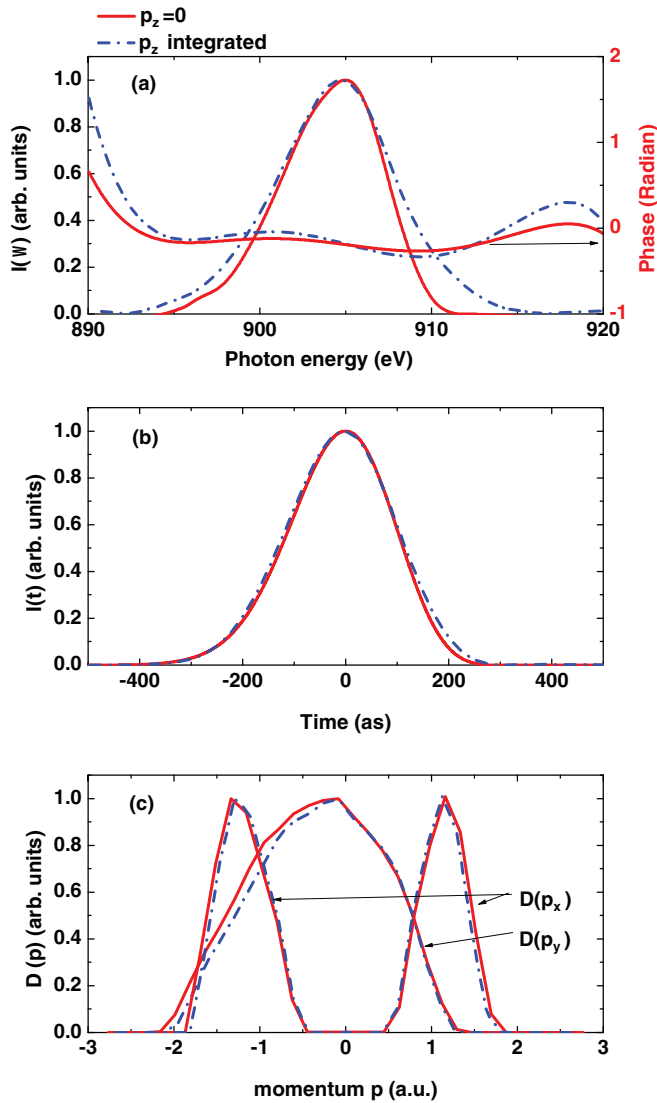


FIG. 12. Dependence of the retrieved quantities using  $S(p_x, p_y)$  spectra with  $p_z = 0$  and by integrating over  $p_z$  as in the experimental data.

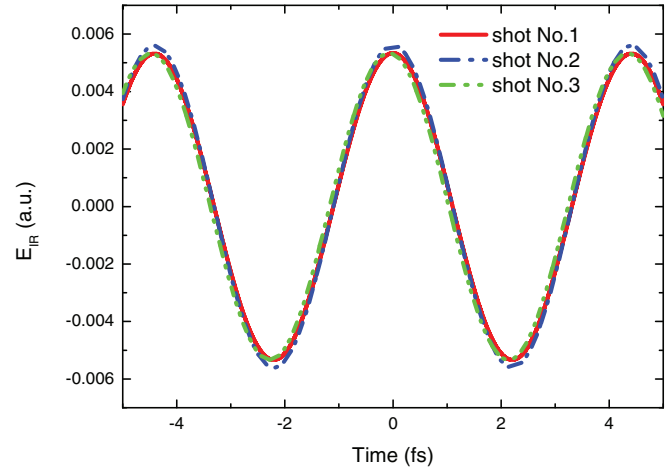


FIG. 13. Retrieved IR fields from three experimental single shots.

incurring much error. Figures 12(a) and 12(b) show, respectively, the spectral and temporal intensities of SXR retrieval using the two different spectra, and the difference is small. The 2D momentum spectra integrated over  $p_y$  and  $p_z$ , as shown in Fig. 12(c), also show little difference. In terms of the FWHM pulse duration, the full calculation obtained a duration of 255 as, compared to 250 as, if only  $p_z = 0$  was used in the retrieval. Thus, we conclude that the  $p_z = 0$  approximation makes a minor difference to the retrieved results, but saves much computing time.

#### 4. IR retrieval

Our method has a capability of retrieving IR from the input spectra. Figure 13 shows three retrieved IR laser fields from three different single-shot experiments; we can see from the figure that the retrieved IR is close to a plane wave. Therefore, it is safe to treat the IR as a plane wave in this calculation, as done in Refs. [15,16]. However, if the IR used in the experiment is not a long-duration pulse, then we cannot set the IR to be directly plane wave. In this case, we need to treat the IR laser field as an unknown function.

- [1] F. Krausz and M. Ivanov, Attosecond physics, *Rev. Mod. Phys.* **81**, 163 (2009).
- [2] T. Popmintchev *et al.*, Bright coherent ultrahigh harmonics in the keV x-ray regime from mid-infrared femtosecond lasers, *Science* **336**, 1287 (2012).
- [3] M.-C. Chen *et al.*, Generation of bright isolated attosecond soft X-ray pulses driven by multicycle midinfrared lasers, *Proc. Natl. Acad. Sci. USA* **111**, E2361 (2014).
- [4] N. Ishii, K. Kaneshima, K. Kitano, T. Kanai, S. Watanabe, and J. Itatani, Carrier-envelope phase-dependent high harmonic generation in the water window using few-cycle infrared pulses, *Nat. Commun.* **5**, 3331 (2014).
- [5] S. L. Cousin, F. Silva, S. Teichmann, M. Hemmer, B. Buades, and J. Biegert, High-flux table-top soft x-ray source driven by sub-2-cycle, CEP stable, 1.85- $\mu\text{m}$  1-kHz pulses for carbon K-edge spectroscopy, *Opt. Lett.* **39**, 5383 (2014).
- [6] C. Ding, W. Xiong, T. Fan, D. D. Hickstein, T. Popmintchev, X. Zhang, M. Walls, M. M. Murnane, and H. C. Kapteyn, High flux coherent super-continuum soft X-ray source driven by a single-stage, 10mJ, Ti:sapphire amplifier-pumped OPA, *Opt. Express* **22**, 6194 (2014).
- [7] K. Hong, C. Lai, J. P. Siqueira, P. Krogen, J. Moses, C. Chang, G. J. Stein, L. E. Zapata, and F. X. Kärtner, Multi-mJ, kHz, 2.1 $\mu\text{m}$  optical parametric chirped-pulse amplifier and high-flux soft x-ray high-harmonic generation, *Opt. Lett.* **39**, 3145 (2014).
- [8] F. Silva, S. M. Teichmann, S. L. Cousin, M. Hemmer, and J. Biegert, Spatiotemporal isolation of attosecond soft X-ray pulses in the water window, *Nat. Commun.* **6**, 6611 (2015).
- [9] J. Li, X. Ren, Y. Yin, Y. Cheng, E. Cunningham, Y. Wu, and Z. Chang, Polarization gating of high harmonic generation in the water window, *Appl. Phys. Lett.* **108**, 231102 (2016).

- [10] S. Hädrich, J. Rothhardt, M. Krebs, S. Demmler, A. Klenke, A. Tünnermann, and J. Limpert, Single-pass high harmonic generation at high repetition rate and photon flux, *J. Phys. B: At. Mol. Opt. Phys.* **49**, 172002 (2016).
- [11] S. B. Zhang, V. Kimberg, and N. Rohringer, Nonlinear resonant Auger spectroscopy in CO using an x-ray pump-control scheme, *Phys. Rev. A* **94**, 063413 (2016).
- [12] J. Li, X. Ren, Y. Yin, K. Zhao, A. Chew, Y. Cheng, E. Cunningham, Y. Wang, S. Hu, Y. Wu, M. Chini, and Z. Chang, 53-attosecond X-ray pulses reach the carbon K-edge, *Nat. Commun.* **8**, 186 (2017).
- [13] T. Gaumnitz, A. Jain, Y. Pertot, M. Huppert, I. Jordan, F. A. Lamas, and H. J. Wörner, Streaking of 43-attosecond soft-x-ray pulses generated by a passively CEP-stable mid-infrared driver, *Opt. Express* **25**, 27506 (2017).
- [14] S. L. Cousin, N. Di Palo, B. Buades, S. M. Teichmann, M. Reduzzi, M. Devetta, A. Kheifets, G. Sansone, and J. Biegert, Attosecond Streaking in the Water Window: A New Regime of Attosecond Pulse Characterization, *Phys. Rev. X* **7**, 041030 (2017).
- [15] J. Duris *et al.*, Tunable isolated attosecond X-ray pulses with gigawatt peak power from a free-electron laser, *Nat. Photon.* **14**, 30 (2020).
- [16] S. Li, Z. Guo, R. N. Coffee, K. Hegazy, Z. Huang, A. Natan, T. Osipov, D. Ray, A. Marinelli, and J. P. Cryan, Characterizing isolated attosecond pulses with angular streaking, *Opt. Express* **26**, 4531 (2018).
- [17] N. Hartmann *et al.*, Attosecond time-energy structure of x-ray free-electron laser pulses, *Nat. Photon.* **12**, 215 (2018).
- [18] M. Hentschel, R. Kienberger, C. Spielmann, G. A. Reider, N. Milosevic, T. Brabec, P. Corkum, U. Heinzmann, M. Drescher, and F. Krausz, Attosecond metrology, *Nature (London)* **414**, 509 (2001).
- [19] X. Zhao, S. J. Wang, W. Yu, H. Wei, C. Wei, B. C. Wang, J. Chen, and C. D. Lin, Metrology of Time-Domain Soft X-Ray Attosecond Pulses and Re-Evaluation of Pulse Durations of Three Recent Experiments, *Phys. Rev. Appl.* **13**, 034043 (2020).
- [20] X. Zhao, H. Wei, Y. Wu, and C. D. Lin, Phase-retrieval algorithm for the characterization of broadband single attosecond pulses, *Phys. Rev. A* **95**, 043407 (2017).
- [21] Y. Mairesse and F. Quéré, Frequency-resolved optical gating for complete reconstruction of attosecond bursts, *Phys. Rev. A* **71**, 011401(R) (2005).
- [22] M. Chini, S. Gilbertson, S. D. Khan, and Z. Chang, Characterizing ultrabroadband attosecond lasers, *Opt. Express* **18**, 13006 (2010).
- [23] P. D. Keathley, S. Bhardwaj, J. Moses, G. Laurent, and F. X. Kärtner, Volkov transform generalized projection algorithm for attosecond pulse characterization, *New J. Phys.* **18**, 073009 (2016).
- [24] Z. Zhu, J. White, Z. Chang, and S. Pang, Attosecond pulse retrieval from noisy streaking traces with conditional variational generative network, *Sci. Rep.* **10**, 5782 (2020).
- [25] J. White and Z. Chang, Attosecond streaking phase retrieval with neural network, *Opt. Express* **27**, 4799 (2019).
- [26] K. Zhao, Q. Zhang, M. Chini, Y. Wu, X. Wang, and Z. Chang, Tailoring a 67 attosecond pulse through advantageous phase-mismatch, *Opt. Lett.* **37**, 3891 (2012).
- [27] W. Helml *et al.*, Measuring the temporal structure of few-femtosecond free-electron laser x-ray pulses directly in the time domain, *Nat. Photon.* **8**, 950 (2014).
- [28] I. Grguraš *et al.*, Ultrafast X-ray pulse characterization at free-electron lasers, *Nat. Photon.* **6**, 852 (2012).
- [29] P. Eckle, M. Smolarski, P. Schlup, J. Biegert, A. Staudte, M. Schöffler, H. G. Müller, R. Dörner, and U. Keller, Attosecond angular streaking, *Nat. Phys.* **4**, 565 (2008).
- [30] W. W. Yu, X. Zhao, H. Wei, S. J. Wang, and C. D. Lin, Method for spectral phase retrieval of single attosecond pulses utilizing the autocorrelation of photoelectron streaking spectra, *Phys. Rev. A* **99**, 033403 (2019).
- [31] X. Zhao, W. Yu, H. Wei, and C. D. Lin, Reconstruction of the complex angle-dependent photoionization transition dipole from a laser-dressed streaking experiment, *Phys. Rev. A* **98**, 053404 (2018).
- [32] X. Zhao, H. Wei, C. Wei, and C. D. Lin, A new method for accurate retrieval of atomic dipole phase or photoionization group delay in attosecond photoelectron streaking experiments, *J. Opt.* **19**, 114009 (2017).
- [33] X. Zhao, S. J. Wang, B. C. Wang, and C. D. Lin, Investigation of isolated attosecond pulse reconstruction from angular integrated photoelectron streaking spectra, *J. Phys.: B.* **53**, 154002 (2020).
- [34] B. C. Wang, L. He, X. Zhao, Y. He, P. Lan, P. Lu, and C. D. Lin, Retrieval of full angular- and energy-dependent complex transition dipoles in molecular frame from laser-induced high-order harmonic signals with aligned molecules, *Phys. Rev. A* **101**, 063417 (2020).
- [35] Z. Zhang, J. Duris, J. P. MacArthur, Z. Huang, and A. Marinelli, Double chirp-taper x-ray free-electron laser for attosecond pump-probe experiments, *Phys. Rev. Accel. Beams* **22**, 050701 (2019).
- [36] M. Lenzen, Ph. Balcou, M. Yu. Ivanov, A. L'Huillier, and P. B. Corkum, Theory of high-harmonic generation by low-frequency laser fields, *Phys. Rev. A* **49**, 2117 (1994).
- [37] Y. T. Zhao, S. C. Jiang, X. Zhao, J. Chen, and Y. Yang, Effect of interband polarization on solid high-order harmonic generation just below band gap, *Opt. Lett.* **45**, 2874 (2020).
- [38] C. Jin, S. J. Wang, X. Zhao, S. F. Zhao, and C. D. Lin, Shaping attosecond pulses by controlling the minima in high-order harmonic generation through alignment of CO<sub>2</sub> molecules, *Phys. Rev. A* **101**, 013429 (2020).
- [39] Y. T. Zhao, X. Xu, S. Jiang, X. Zhao, J. G. Chen, and Y. J. Yang, Cooper minimum of high-order harmonic spectra from MgO crystal in an ultrashort laser pulse, *Phys. Rev. A* **101**, 033413 (2020).
- [40] Y. T. Zhao, S. Y. Ma, S. C. Jiang, Y. J. Yang, X. Zhao, and J. G. Chen, All-optical reconstruction of  $k$ -dependent transition dipole moment by solid harmonic spectra from ultrashort laser pulses, *Opt. Express* **27**, 34392 (2019).
- [41] J. Zhang, X. F. Pan, X. Zhao, J. Guo, K. G. Zhu, and X. S. Liu, Spectral splitting and phase matching of the macroscopic high-order harmonic generation in intense laser fields, *J. Opt.* **21**, 125503 (2019).